Commun Nonlinear Sci Numer Simulat 139 (2024) 108292

Contents lists available at ScienceDirect

Communications in Nonlinear Science and Numerical Simulation

journal homepage: www.elsevier.com/locate/cnsns

Research paper

Is maximum tolerated dose (MTD) chemotherapy scheduling optimal for glioblastoma multiforme?

Chiu-Yen Kao [a,1], Seyyed Abbas Mohammadi [b,c,*], Mohsen Yousefnezhad [d,2]

[a] Department of Mathematical Sciences, Claremont McKenna College, 850 Columbia Ave, Claremont, CA 91711, United States of America
[b] Division of Mathematics, University of Dundee, Dundee DD1 4HN, United Kingdom
[c] School of Computer Science and Applied Mathematics, University of The Witwatersrand, Braamfontein, 2000, Johannesburg, South Africa
[d] Department of Mathematics, Collage of Sciences, Shiraz University, Fars, Iran

ARTICLE INFO

Keywords:
Optimal control of PDEs
Chemotherapy scheduling
Analytical solution
Bang-bang solution
Glioblastoma multiforme

ABSTRACT

In this study, we investigate a control problem involving a reaction–diffusion partial differential equation (PDE). Specifically, the focus is on optimizing the chemotherapy scheduling for brain tumor treatment to minimize the remaining tumor cells post-chemotherapy. Our findings establish that a bang-bang increasing function is the unique solution, affirming the MTD scheduling as the optimal chemotherapy profile. Several numerical experiments on a real brain image with parameters from clinics are conducted for tumors located in the frontal lobe, temporal lobe, or occipital lobe. They confirm our theoretical results and suggest a correlation between the proliferation rate of the tumor and the effectiveness of the optimal treatment.

1. Introduction

Glioblastoma multiforme (GBM) is an extremely invasive brain tumor, typically associated with life expectancies ranging from 6 to 12 months [1–3]. Chemotherapy is an essential aspect of postoperative treatments. After undergoing surgery for diagnostic and therapeutic purposes, patients often face the recurrence of tumors, necessitating postoperative strategies like radiotherapy and chemotherapy to mitigate tumor progression [4–6]. Developing optimized chemotherapy scheduling is imperative to enhance conventional treatments and increase patient survival rates.

In regular chemotherapy plans, medications are given using MTD, with breaks for rest periods in between when patient recover from side effects. This raises the question of whether this chemotherapy scheduling is optimal, meaning it results in fewer surviving tumor cells [5,7,8]. To investigate this, a mathematical model for tumor evolution during therapy is essential. Deterministic models based on reaction–diffusion partial differential equations (PDEs) provide a suitable tool for studying patient-specific tumor kinetics observed on magnetic resonance imaging (MRI). These models have been developed during the past decades and shown success in determining the patients probable to benefit from extensive surgery, quantifying treatment response using untreated virtual controls, estimated survival time for the patients, the effect of chemotherapy on tumor growth, and some other aspects, see [6,9–11] and the references there in. The PDE models are based on parameters such as dispersal or diffusion rate, proliferation rate, and the spatial distribution of tumor cells, all of which can be obtained for each patient using MRIs.

In this paper, we employ a variant of the model developed in [9] and the references therein to address the question of determining optimal chemotherapy scheduling. Several researchers have addressed the question of optimal chemotherapy profiles, with most of

* Corresponding author at: Division of Mathematics, University of Dundee, Dundee DD1 4HN, United Kingdom.
E-mail addresses: ckao@cmc.edu (C.-Y. Kao), smohammadi001@dundee.ac.uk, abbas.mohammadi@wits.ac.za (S.A. Mohammadi), m.yousefnezhad@shirazu.ac.ir (M. Yousefnezhad).

[1] The work of this author was partially supported by NSF grant DMS-2208373.
[2] The work of this author is based upon research funded by Iran National Science Foundation (INSF) under project No. 4024073.

https://doi.org/10.1016/j.cnsns.2024.108292
Received 22 June 2024; Accepted 20 August 2024
Available online 28 August 2024

them considering ordinary differential equations to model the evolution of tumors during treatment. However, this approach often leads to neglecting the essential characteristic of GBM, which is its invasion into neighboring tissue, [12–16], to name just a few. To consider the invasion or diffusion of the tumor, PDEs should be used to model its behavior [17]. Recently the authors of [16] employed a reaction–diffusion PDE to examine the temporal behavior of GBM in the presence of chemotherapy. The study addressed the question of determining optimal chemotherapy strategies to inhibit the growth of GBM. The authors formulated the problem as an optimal control problem for a reaction–diffusion PDE. The objective function was defined as the total population size of the tumor throughout a cycle of chemotherapy. Using a gradient based numerical method, the authors showed that a MTD type scheduling which starts at the maximum dose and terminates with a rest period is a (local) optimizer.

The formulation of the objective function as the total population size of the tumor in a cycle of chemotherapy, while mathematically tractable, may lack practical relevance from a biological standpoint. In clinical contexts, the significance often lies in the number of tumors at the end of the cycle which is an indicator of survival for a patient [7,8,17]. In this study we consider the population size of the tumor on the final day of the cycle as the objective function. While [16] considered a homogeneous drug delivery to brain tissue, in this paper we consider heterogeneous drug delivery to GBM, a more biologically relevant scenario. As it is computationally intensive to perform many real brain simulations, we analytically determine the global optimizer, which corresponds to the current practice of MTD-type scheduling in clinics. It is noteworthy that obtaining analytical solutions in the context of optimal control for PDEs is quite rare [18]. Deriving analytical formulas for chemotherapy profiles is a novel development in this context.

Moreover, we consider the PDE in a more general form compared to what was considered in [6,10,11,16]. This general form allows for the consideration of more complex models for brain tumors, taking into account the intricacies of tumor growth dynamics within the brain.

Our optimal chemotherapy profile suggests a "bang–bang" strategy, commencing at a rest period and concluding with the maximum allowable dose. It is the profile that is now using in clinics, see for example [17, Section 11]. Although the results of [16] also suggest a bang–bang profile, it is not the optimal strategy while we want to minimize the population size of the tumor at the end of a cycle of chemotherapy. Furthermore, based upon the model we have considered, our findings indicate that the optimal strategy is unique, with no room for further improvement. Our results also serve as a new validation for the models proposed in [9,17] in studying tumor behavior. By considering the optimal strategy alongside alternative scheduling approaches, we numerically solve (1) on an actual brain image to compute tumor cell density and total population size at the end of the chemotherapy cycle. Various tumor locations are examined, and computations utilize parameters sourced from clinical data. These analyses yield insights into treatment efficacy.

The organization of the paper is as follows. In Section 2, a mathematical formulation of the tumor growth subjects to a chemotherapy treatment is presented. The existence of an optimal solution is established in Section 3 and the optimal chemotherapy scheduling is derived in Section 4. We perform numerical calculations and report the results in Section 5 which provide insights into treatment efficacy. In Section 6, we conclude our findings and discuss possible future directions.

2. Mathematical formulation

This section is dedicated to the mathematical formulation of the optimal chemotherapy profile as an optimal control problem for a PDE.

Let $\mathcal{B} \subset \mathbb{R}^n$ be the brain domain with smooth boundary. Let $u(\mathbf{x}, t)$ be the density of brain tumor cells in $\mathbf{x}$ at the moment t and $\mathbf{n}$ be the outer normal unit vector to $\partial\mathcal{B}$. We will consider the following model describing the growth of the brain tumor cell population under the influence of chemotherapy [10],

$$\begin{cases} \partial_t u - \nabla \cdot (D(\mathbf{x})\nabla u) = \rho(\mathbf{x})u\left(1 - \dfrac{u}{K(\mathbf{x})}\right) - C(t)\eta(\mathbf{x})u, & (\mathbf{x}, t) \in \mathcal{B} \times (0, T), \\ \partial_{\mathbf{n}} u = 0, & (\mathbf{x}, t) \in \partial\mathcal{B} \times (0, T), \\ u(\mathbf{x}, 0) = u_0(\mathbf{x}), & \mathbf{x} \in \mathcal{B}, \end{cases} \tag{1}$$

where $0 < D(\mathbf{x}) \in L^\infty(\mathcal{B})$, is the diffusion coefficient or invasion rate, $0 < \rho(\mathbf{x}) \in L^\infty(\mathcal{B})$ is proliferation rate, and $0 < K(\mathbf{x}) \in L^\infty(\mathcal{B})$ represents the carry capacity of the tissue, which provides an upper limit on the number of tumor cells capable of occupying any cubic millimeter of brain.

It should be noted that one of the most significant aspects of (1) is its consideration of the heterogeneous structure of brain tissue. Experimental observations have shown that glioma cells migrate more rapidly in white matter than in the gray matter of the human brain. This observation justifies the consideration of D as a function of space $\mathbf{x}$, such that $D(\mathbf{x}) = D_g$ in gray matter and $D(\mathbf{x}) = D_w$ in white matter. Let $\mathcal{B}_g$ stands for the gray matter region and $\mathcal{B}_w$ white matter region, respectively. Then, $\mathcal{B}_w$ and $\mathcal{B}_g$ form a partition of brain $\mathcal{B}$, i.e., $\mathcal{B}_w \cup \mathcal{B}_g = \mathcal{B}$ and $\mathcal{B}_w \cap \mathcal{B}_g = \emptyset$ [17]. Therefore, we have

$$D(\mathbf{x}) := \begin{cases} D_g & \text{if } \mathbf{x} \in \mathcal{B}_g, \\ D_w & \text{if } \mathbf{x} \in \mathcal{B}_w, \end{cases}$$

with $D_w > D_g > 0$.

In (1), the function $C(t)$ denotes the proportion of dose delivery or chemotherapy effort to patient at time t. For example, $C(t) = 0, 0.5, 1$ indicate no drug delivery, half dose and full dose administration, respectively. In this way, $C(t)$ shows the temporal

profile of chemotherapy applied to a patient for $t \in (0,T)$, where T is the length of a single cycle of chemotherapy. In this paper, we incorporate the effects of heterogeneity in the vascular structure of brain tissue, resulting in heterogeneous drug delivery [10]. To account for this heterogeneity, we introduce the function $\eta(\mathbf{x})$ in the model, defined as

$$\eta(\mathbf{x}) := \begin{cases} C_g & \text{if } \mathbf{x} \in \mathcal{B}_g, \\ C_w & \text{if } \mathbf{x} \in \mathcal{B}_w, \end{cases}$$

where C_g and C_w represent the effectiveness of chemotherapy reaching the brain tissue, with the maximum allowable dose administered in the gray matter region $\mathcal{B}_g$ and the white matter region $\mathcal{B}_w$, respectively. The function $u_0(\mathbf{x})$ represents the density of tumor cells at the onset of treatment.

In light of the clinical chemotherapy limits ensuring patient safety, the chemotherapy function $C(t)$ and its cumulative amount $\int_0^T C(t)dt$ satisfy the following properties:

$$0 \le C(t) \le 1, \quad \text{for} \quad 0 \le t \le T, \quad \text{and} \quad \int_0^T C(t)dt = \gamma, \tag{2}$$

where $0 < \gamma < T$ represents the total amount of chemotherapy effort in a cycle of chemotherapy. So, we define the admissible set as

$$\mathcal{A} = \{C \in L^\infty(0,T) : \quad (2) \text{ holds } \},$$

consisting all possible chemotherapy profile.

Our goal is to determine optimal chemotherapy strategies that result in the smallest tumor population at the end of a chemotherapy cycle. Mathematically, one should consider

$$J(C) = \int_{\mathcal{B}} u_C(\mathbf{x}, T)d\mathbf{x},$$

where we use the notation u_C to emphasize the solution u of (1) depends on C. Then, $J(C)$ represents the total population of tumor cells at the final time T as our objective functional and we should find a solution for

$$\min_{C \in \mathcal{A}} J(C). \tag{3}$$

The solution of (3) yields the optimal chemotherapy scheduling, resulting in the lowest amount of tumor cells at the end of treatment.

3. Existence of an optimal solution

To determine the optimal solution of (3), we first need to establish the existence of such a solution. To do so, we require a mathematical framework and specific notations.

We begin by introducing a space of functions that will be utilized throughout the paper. The set $H^1(\mathcal{B})$ consists of functions whose function and weak derivatives belong to $L^2(\mathcal{B})$. The dual space of $H^1(\mathcal{B})$, denoted as $H^1(\mathcal{B})^*$, is then defined. The set of functions $L^2\left(0,T;H^1(\mathcal{B})\right)$ is defined as the set of functions $u : [0,T] \to H^1(\mathcal{B})$ such that

$$\|u\|_{L^2(0,T;H^1(\mathcal{B}))} := \left(\int_0^T \|u(.,t)\|^2_{H^1(\mathcal{B})} dt\right)^{\frac{1}{2}} < \infty.$$

By replacing the norm in this definition with the norm of $H^1(\mathcal{B})^*$, we obtain the definition of $L^2\left(0,T;H^1(\mathcal{B})^*\right)$. A function $u : [0,T] \to H^1(\mathcal{B})$ belongs to $L^\infty\left(0,T;H^1(\mathcal{B})\right)$ if

$$\|u\|_{L^\infty(0,T;H^1(\mathcal{B}))} := \operatorname*{ess\,sup}_{0\le t\le T} \|u(.,t)\|_{H^1(\mathcal{B})} < \infty.$$

The space $C([0,T];H^1(\mathcal{B}))$ is defined as the set of continuous functions $u : [0,T] \to H^1(\mathcal{B})$ such that

$$\|u\|_{C([0,T];H^1(\mathcal{B}))} := \sup_{0\le t\le T} \|u(x,.)\|_{H^1(\mathcal{B})} < \infty.$$

For more information on these function spaces, refer for instance to [19].

Now, we define the solution of (1) in the weak sense as follows.

Definition 1. We say a function $u \in L^2\left(0,T;H^1(\mathcal{B})\right)$ with $u_t \in L^2\left(0,T;H^1(\mathcal{B})^*\right)$ and $u(\mathbf{x},0) = u_0(\mathbf{x})$ is a weak solution of (1) if

$$\int_{\mathcal{B}} \partial_t u\phi \; d\mathbf{x} + \int_{\mathcal{B}} D(\mathbf{x})\nabla u \cdot \nabla\phi \; d\mathbf{x} = \int_{\mathcal{B}} \left(\rho(\mathbf{x})u\left(1 - \frac{u}{K(\mathbf{x})}\right) - C(t)\eta(\mathbf{x})u\right)\phi \; d\mathbf{x}, \tag{4}$$

for all $\phi \in H^1(\mathcal{B})$ and almost every $0 \le t \le T$.

The existence, uniqueness, and nonnegativity of the solution to problem (1) is classical and one can find a proof for instance in [18–21]. Moreover, it is straightforward to show that there exists a positive constant A independent of u and C such that

$$\|u\|_{L^\infty(0,T;L^2(\mathcal{B}))} + \|u\|_{L^2(0,T;H^1(\mathcal{B}))} + \|\partial_t u\|_{L^2(0,T;H^1(\mathcal{B})^*)} \le A, \tag{5}$$

where A is a generic constant in this paper. In view of the fact that $u \in L^2(0,T;H^1(\mathcal{B}))$ and $u_t \in L^2(0,T;H^1(\mathcal{B})^*)$, we infer that $u \in C([0,T];L^2(\mathcal{B}))$ [18,19,21]. Moreover, in view of [22, Theorem 3.1], we find that if $u_0 \in H^1(\mathcal{B})$, then $u(x,t)$ is a bounded function on $\mathcal{B}_T := \mathcal{B} \times (0,T)$, or there exists $A > 0$ such that $\|u\|_{L^\infty(\mathcal{B}_T)} \le A$ where A depends solely on $\|D\|_{L^\infty}$, $\|\eta\|_{L^\infty}$, $|\mathcal{B}|$, T, n, $\|\rho\|_{L^\infty(\mathcal{B})}$, $\|K\|_{L^\infty(\mathcal{B})}$, and $\|u_0\|_{L^\infty(\mathcal{B})}$.

Mathematically, the first question in addressing an optimization problem is to determine the existence of a solution within the admissible set of functions. We address the existence of a solution for the minimization problem (3). This existence can be demonstrated through the application of the standard variational method, detailed in references such as [18,19].

Theorem 1. *Assume that $u_0 \in H^1(\mathcal{B})$. There is $C^\star \in \mathcal{A}$ with $u^\star := u_{C^\star}$ such that*

$$J(C^\star) \le J(C), \quad \textit{for all} \quad C \in \mathcal{A},$$

i.e., problem (3) has a solution.

Proof. Recall that $J(C) \ge 0$ for every $C \in \mathcal{A}$ in view of the non-negativity of u_C. Define $0 \le \hat{J} = \inf_{C\in\mathcal{A}} J(C)$, and consider a minimizing sequence $\{C_k\}_1^\infty$ such that $\lim_{k\to\infty} J(C_k) = \hat{J}$. Set $u_k := u_{C_k}$. Invoking (5) we have

$$\|u_k\|_{L^\infty(0,T;L^2(\mathcal{B}))} + \|u_k\|_{L^2(0,T;H^1(\mathcal{B}))} + \|\partial_t u_k\|_{L^2(0,T;H^1(\mathcal{B})^*)} \le A, \quad \text{for} \quad k = 1,2,3,\dots. \tag{6}$$

In view of (6) and by passing to a sub-sequence, it is inferred that there is $u^\star \in L^2(0,T;H^1(\mathcal{B}))$ such that

$$u_k \rightharpoonup u^\star \quad \text{weakly in} \quad L^2(0,T;H^1(\mathcal{B})), \tag{7}$$

$$\partial_t u_k \rightharpoonup \partial_t u^\star \quad \text{weakly in} \quad L^2(0,T;H^1(\mathcal{B})^*), \tag{8}$$

$$u_k \to u^\star \quad \text{strongly in} \quad L^2(\mathcal{B}_T). \tag{9}$$

Remember that $\{C_k\}_1^\infty$ is a bounded sequence in $L^\infty(0,T)$, see (2). Passing to a sub-sequence, there is $C^\star \in L^\infty(0,T)$ such that

$$C_k \rightharpoonup C^\star \quad \text{with respect to the weak star topology on} \quad L^\infty(0,T). \tag{10}$$

We show that indeed $C^\star \in \mathcal{A}$. In view of (10), it is concluded that $\int_0^T C^\star(t)dt = \gamma$. Let $B = \{t \in [0,T] : \ C^\star(t) > 1\}$ and let $|B| > 0$. Due to the fact that $C_k(t) \le 1$ almost everywhere in $[0,T]$ and (10), one can see that

$$0 < \int_0^T \left(C^\star(t) - 1\right) \chi_B(t)dt = \lim_{k\to\infty} \int_0^T \left(C_k(t) - 1\right) \chi_B(t)dt \le 0,$$

which is a contradiction. Consequently, we infer $C^\star(t) \le 1$ in $[0,T]$. A similar argument demonstrates that $C^\star(t) \ge 0$ for $t \in [0,T]$. Hence, we conclude that $C^\star$ belongs to $\mathcal{A}$.

Next step is to show that $u^\star$ is the unique solution of (1) corresponding to $C^\star$. It is obvious that for any $\phi \in H^1(\mathcal{B}_T)$, u_k satisfies

$$\int_{\mathcal{B}_T} \partial_t u_k \phi \ d\mathbf{x}dt + \int_{\mathcal{B}_T} D(\mathbf{x})\nabla u_k \cdot \nabla\phi \ d\mathbf{x}dt = \int_{\mathcal{B}_T} \left(\rho - C_k(t)\eta(\mathbf{x})\right) u_k \phi d\mathbf{x}dt - \int_{\mathcal{B}_T} \left(\frac{\rho}{K(\mathbf{x})}\right) u_k^2 \phi d\mathbf{x}dt.$$

Passing $k \to \infty$, we observe that

$$\int_{\mathcal{B}_T} \partial_t u^\star \phi \ d\mathbf{x}dt + \int_{\mathcal{B}_T} D(\mathbf{x})\nabla u^\star \cdot \nabla\phi \ d\mathbf{x}dt = \int_{\mathcal{B}_T} \left(\rho(\mathbf{x})u^\star \left(1 - \frac{u^\star}{K(\mathbf{x})}\right) - C^\star(t)\eta(\mathbf{x})u^\star\right) \phi d\mathbf{x}dt, \tag{11}$$

in view of (7)–(9). It is classic that the variational form in (11) is equivalent to the variational form in Definition 1, see for instance [19], and so $u^\star = u_{C^\star}$.

The last step is to show that $C^\star$ is a minimizer. Let us define $f_k(t) := \|u_k(.,t) - u^\star(.,t)\|^2_{L^2(\mathcal{B})} \ge 0$. From the continuity of solutions of (1) with respect to time and (9) we have

$$f_k \in C[0,T], \qquad \text{and} \qquad f_k \longrightarrow 0 \quad \text{strongly in} \quad L^1(0,T). \tag{12}$$

According to (12), there exists a sub-sequence of f_k, still denoted by f_k for simplicity, that $f_k \longrightarrow 0$ for all $t \in [0,T]$ and consequently $u_k(\cdot,T) \longrightarrow u^\star(\cdot,T)$ strongly in $L^2(\mathcal{B})$. This yields that

$$\hat{J} = \lim_{k\to\infty} J(C_k) = \lim_{k\to\infty} \int_{\mathcal{B}} u_k(\mathbf{x},T) \ d\mathbf{x} = \int_{\mathcal{B}} u^\star(\mathbf{x},T) \ d\mathbf{x} = J(C^\star), \tag{13}$$

and so $C^\star$ is a solution for the optimization problem (3). □

4. Determining the optimal chemotherapy profile

In this section we address the question of finding an analytical solution for (3). It is worth noting that obtaining analytical solutions for PDE-constrained optimization problems is uncommon. Typically, such solutions require prior knowledge of the optimizer, which is often not available. We will calculate the solution which is the optimal chemotherapy scheduling that minimizes the population size of the tumor on the last day of the chemotherapy cycle. To accomplish this, we first establish an adjoint equation.

Then, utilizing its solution, the adjoint state, we derive a necessary optimality condition which furnishes us with the information needed to determine the optimal solution. To have more information regarding this approach refer to [18].

For $C \in \mathcal{A}$, let $p(\mathbf{x},t)$ represent the adjoint state where satisfies the following PDE, which we refer to as the adjoint equation.

$$\begin{cases} \partial_t p + \nabla\cdot(D(\mathbf{x})\nabla p) + \left(\rho(\mathbf{x}) - \dfrac{2\rho(\mathbf{x})}{K(\mathbf{x})}u - C(t)\eta(\mathbf{x})\right)p = 0 & \text{in} \quad \mathcal{B}\times(0,T), \\ \dfrac{\partial p}{\partial \mathbf{n}} = 0 & \text{on} \quad \partial\mathcal{B}\times(0,T), \\ p(\mathbf{x},T) = 1 & \text{in} \quad \mathcal{B}. \end{cases} \tag{14}$$

In (14), $u = u_C$ is the solution of (1) corresponding to C. Eq. (14) has a unique solution in the weak sense defined in Definition 1, [18–21].

Lemma 1. *Let $C \in \mathcal{A}$ and consider $u = u_C$ be the corresponding solution of (1). There exists a nonnegative weak solution $p \in L^2\left(0,T;H^1(\mathcal{B})\right)$ with $\partial_t p \in L^2\left(0,T;H^1(\mathcal{B})^*\right)$ for the problem (14).*

Now we need a sensitivity analysis of our problem. Let $\epsilon > 0$, $h \in L^\infty(0,T)$ be given such that $C_\epsilon = C + \epsilon h \in \mathcal{A}$ for small enough ϵ. Denote by u and u_ϵ the solutions of problem (1) associated with C and C_ϵ respectively. Setting $w_\epsilon = (u_\epsilon - u)/\epsilon$, it is straightforward to check that w_ϵ is the weak solution of

$$\begin{cases} \partial_t w_\epsilon - \nabla\cdot\left(D(\mathbf{x})\nabla w_\epsilon\right) - \left(\rho(\mathbf{x}) - \dfrac{2\rho(\mathbf{x})}{K(\mathbf{x})}u_\epsilon - C\eta(\mathbf{x})\right)w_\epsilon = -h\eta(\mathbf{x})u_\epsilon & \text{in} \quad \mathcal{B}\times(0,T), \\ \dfrac{\partial w_\epsilon}{\partial \mathbf{n}} = 0 & \text{on} \quad \partial\mathcal{B}\times(0,T), \\ w_\epsilon(\mathbf{x},0) = 0 & \text{in} \quad \mathcal{B}. \end{cases} \tag{15}$$

Similar to the proof of Theorem 1, we can show that $\lim_{\epsilon\to 0} u_\epsilon = u_C$ in the weak scenes in $L^2(0,T;H^1(\mathcal{B}))$. In view of this fact, we establish the following lemma.

Lemma 2. *There exists function w such that $\lim_{\epsilon\to 0} w_\epsilon = w$ in the weak scenes in $L^2(0,T;H^1(\mathcal{B}))$. In addition, w is the unique weak solution of*

$$\begin{cases} \partial_t w - \nabla\cdot(D(\mathbf{x})\nabla w) - \left(\rho(\mathbf{x}) - \dfrac{2\rho(\mathbf{x})}{K(\mathbf{x})}u - C\eta(\mathbf{x})\right)w = -h\eta(\mathbf{x})u & \textit{in} \quad \mathcal{B}\times(0,T), \\ \dfrac{\partial w}{\partial \mathbf{n}} = 0 & \textit{on} \quad \partial\mathcal{B}\times(0,T), \\ w(\mathbf{x},0) = 0 & \textit{in} \quad \mathcal{B}, \end{cases} \tag{16}$$

where $u = u_C$.

Proof. If we show that there exists a constant $A > 0$ such that

$$\|w_\epsilon\|_{L^2(0,T;H^1(\mathcal{B}))} \le A, \tag{17}$$

$$\|\partial_t w_\epsilon\|_{L^2(0,T;H^1(\mathcal{B})^*)} \le A, \tag{18}$$

then we can conclude that there is a sub-sequence, let say w_{ϵ_i}, and $w \in L^2\left(0,T;H^1(\mathcal{B})\right)$ such that

$$w_{\epsilon_i} \rightharpoonup w \quad \text{weakly in} \quad L^2(0,T;H^1(\mathcal{B})), \tag{19}$$

$$\partial_t w_{\epsilon_i} \rightharpoonup \partial_t w \quad \text{weakly in} \quad L^2(0,T;H^1(\mathcal{B})^*). \tag{20}$$

Whenever we have (19)–(20), then similar to that in the proof of Theorem 1, one can conclude that w is the solution of (16) in the weak sense.

We start by establishing (17). Multiplying both sides of (15) by w_ϵ and integrating yields

$$\frac{1}{2}\|w_\epsilon\|^2_{L^2(\mathcal{B})} + D_g\int_0^t \|\nabla w_\epsilon\|^2_{L^2(\mathcal{B})}dt \le \|\rho\|_{L^\infty(\mathcal{B})}\int_0^t \|w_\epsilon\|^2_{L^2(\mathcal{B})}dt + \|h\eta u_\epsilon\|_{L^\infty(\mathcal{B})}\int_0^t\int_{\mathcal{B}} |w_\epsilon|dtd\mathbf{x}, \tag{21}$$

for all $0 \le t \le T$. Now employing the inequality $ab \le (a^2+b^2)/2$ for real numbers a, b for the last integral, we arrive at the following inequality

$$\frac{1}{2}\|w_\epsilon\|^2_{L^2(\mathcal{B})} + D_g\int_0^t \|\nabla w_\epsilon\|^2_{L^2(\mathcal{B})}dt \le \|\rho\|_{L^\infty(\mathcal{B})}\int_0^t \|w_\epsilon\|^2_{L^2(\mathcal{B})}dt + \frac{\|h\eta u_\epsilon\|_{L^\infty(\mathcal{B})}}{2}\left(T|\mathcal{B}| + \int_0^t \|w_\epsilon\|^2_{L^2(\mathcal{B})}dt\right), \tag{22}$$

which yields that

$$\|w_\epsilon\|^2_{L^2(\mathcal{B})} \le A_1\int_0^t \|w_\epsilon\|^2_{L^2(\mathcal{B})}dt + A_2, \quad \text{for all} \quad 0 \le t \le T,$$

where A_1 and A_2 are positive constants independent of t. Now, in view of this inequality and Grönwall's inequality, one can infer that

$$\|w_\epsilon\|_{L^2(\mathcal{B})} \le A, \tag{23}$$

Inequalities (22)–(23) leads us to the fact that

$$\int_0^t \|\nabla w_\epsilon\|^2_{L^2(\mathcal{B})} dt \le A, \quad \text{for all} \quad 0 \le t \le T,$$

and so $\|w_\epsilon\|_{L^2(0,T;H^1(\mathcal{B}))} \le A$ where A is a constant independent of ϵ. This completes the proof of (17).

To prove (18), we multiply both sides of (15) by a test function $\phi \in L^2\left(0,T;H^1(\mathcal{B})\right)$ and integrate such that

$$\int_0^t \int_{\mathcal{B}} \partial_t w_\epsilon \phi d\mathbf{x}dt = -\int_0^t \int_{\mathcal{B}} D\nabla w_\epsilon \cdot \nabla\phi d\mathbf{x}dt + \int_0^t \int_{\mathcal{B}} \left(\rho(\mathbf{x}) - \frac{2\rho(\mathbf{x})}{K(\mathbf{x})} u_\epsilon - C\eta(\mathbf{x})\right) w_\epsilon \phi d\mathbf{x}dt - \int_0^t \int_{\mathcal{B}} h\eta u_\epsilon \phi d\mathbf{x}dt.$$

In view of (17) and (23), it is straightforward to conclude from the last equation that

$$\left|\int_0^t \int_{\mathcal{B}} \partial_t w_\epsilon \phi d\mathbf{x}dt\right| \le A\|\phi\|_{L^2(0,T;H^1(\mathcal{B}))},$$

which leads to

$$\|\partial_t w_\epsilon\|_{L^2(0,T;H^1(\mathcal{B})^*)} < A,$$

where A is a constant independent of ϵ. This is the proof for (18). □

We need the following technical lemmas to determine the optimal chemotherapy.

Lemma 3. *(i) Let u be the solution for Eq. (1). Then*

$$\int_{\mathcal{B}} u(\mathbf{x},t)\, d\mathbf{x} \ge e^{-\alpha T} \int_{\mathcal{B}} u_0(\mathbf{x})\, d\mathbf{x} \tag{24}$$

for each $0 \le t \le T$, where $\alpha = \|u\|_{L^\infty(\mathcal{B}_T)} \|\frac{\rho}{K}\|_{L^\infty(\mathcal{B})} + \|\eta\|_{L^\infty(0,T)}$. (ii) Let p be the solution of the adjoint PDE (14). Then, we have

$$\int_{\mathcal{B}} p(\mathbf{x},t)\, d\mathbf{x} \ge e^{-T\|\rho\|_{L^\infty(\mathcal{B})}} \int_{\mathcal{B}} p(\mathbf{x},0) d\mathbf{x}, \qquad \text{for each} \quad 0 \le t \le T. \tag{25}$$

Proof. (i) Let $t \in [0,T]$, and $I(s) := \int_{\mathcal{B}} u(\mathbf{x},s)\, d\mathbf{x}$; then from (4) for $\phi \equiv 1$ we get

$$I'(s) = \int_{\mathcal{B}} u_s\, d\mathbf{x} = \int_{\mathcal{B}} \left(\rho(\mathbf{x})u\left(1 - \frac{u}{K(\mathbf{x})}\right) - C(s)\eta(\mathbf{x})u\right) d\mathbf{x} \ge -\int_{\mathcal{B}} \left(\frac{\rho(\mathbf{x})u}{K(\mathbf{x})} + C(s)\eta(\mathbf{x})\right) u\, d\mathbf{x} \ge -\alpha I(s),$$

for a.e., $0 \le s \le T$. Then, Grönwall's inequality yields $I(t) \ge e^{-\alpha t} I(0)$ which implies (24). (ii) The reasoning is similar to that of part (i) and we omit it. □

Now we can determine the unique analytical solution for (3). The next theorem provides a practically implementable formula for the optimal profile of chemotherapy.

Theorem 2. *Let $C^\star \in \mathcal{A}$ represent a solution for problem (3). Then we have*

$$C^\star(t) = \begin{cases} 0 & \text{if} \quad 0 \le t < T - \gamma \\ 1 & \text{if} \quad T - \gamma \le t \le T. \end{cases} \tag{26}$$

In particular, the solution is unique.

Proof. Let $u = u_{C^\star}$. Assume p is the adjoint state, the solution of (14), corresponding to $C^\star$, and w is the solution of (16) corresponding to $C^\star$. Multiply both sides of (14) by w and multiply both sides of (16) by p. Now integrate both resulting equations with respect to time and space over $\mathcal{B}$. Add the resulting equations, it is easily verified that

$$\int_{\mathcal{B}} w(\mathbf{x},T)\, d\mathbf{x} = -\int_0^T \int_{\mathcal{B}} h\eta p u\, d\mathbf{x}dt. \tag{27}$$

Let $h \in L^\infty(0,T)$ be given such that $C^\star + \epsilon h \in \mathcal{A}$ for small enough ϵ. In view of Lemma 2, it is straightforward to calculate the Gâteaux derivative of the cost functional $J(C)$ at $C^\star$ in the following form

$$(J'(C^\star), h)_{L^2(0,T)} = \lim_{\epsilon \to 0} \frac{J(C^\star + \epsilon h) - J(C^\star)}{\epsilon} = \int_{\mathcal{B}} w(\mathbf{x},T)\, d\mathbf{x}$$

$$= -\int_0^T h(t)\left(\int_{\mathcal{B}} \eta(.)p(\cdot,t)u(\cdot,t)\,d\mathbf{x}\right)dt = -\int_0^T h(t)\Psi(t)dt, \tag{28}$$

where $\Psi(t) := \int_{\mathcal{B}} \eta(.)p(\cdot,t)u(\cdot,t)\,d\mathbf{x}$. This reveals that for a minimizer $C^\star$ we have

$$J\left(C^\star + \epsilon\left(C - C^\star\right)\right) - J\left(C^\star\right) = \epsilon\int_0^T \left(C^\star - C\right)\Psi(t)dt + o(\epsilon), \quad \text{as} \quad \epsilon \to 0,$$

and so we obtain

$$\int_0^T C^\star\Psi(t)dt - \int_0^T C\Psi(t)dt \geq 0, \quad \text{for all} \quad C \in \mathcal{A},$$

which means that any minimizer of (3) is a maximizer of the linear functional $\mathcal{L}(C) := \int_0^T C(t)\Psi(t)dt$ for $C \in \mathcal{A}$.

One can observe that for any admissible control C we have

$$\begin{aligned}\frac{\Psi(t)}{dt} &= \int_{\mathcal{B}} \eta\left(u\partial_t p\,d\mathbf{x} + \int_{\mathcal{B}} p\partial_t u\right)d\mathbf{x}\\ &= \int_{\mathcal{B}}\left(-\nabla\cdot(D(\mathbf{x})\nabla p) - \left(\rho(\mathbf{x}) - \frac{2\rho(\mathbf{x})}{K(\mathbf{x})}u - C\eta\right)p\right)u\eta\,d\mathbf{x}\\ &+ \int_{\mathcal{B}}\left(\nabla\cdot(D(\mathbf{x})\nabla u) + \left(\rho(\mathbf{x}) - \frac{\rho(\mathbf{x})}{K(\mathbf{x})}u - C\eta\right)u\right)p\eta\,d\mathbf{x} = \int_{\mathcal{B}} \eta(\mathbf{x})\frac{\rho(\mathbf{x})}{K(\mathbf{x})}pu^2\,d\mathbf{x} > 0,\end{aligned}$$

where the last inequality is obtained in view of (24) and (25). This means that $\Psi(t)$ is strictly increasing in t.

In view of strict monotonicity of Ψ, we show that function $C^\star$ with formula (26) is the unique maximizer of $\mathcal{L}(C)$ for $C \in \mathcal{A}$ and so it is the unique minimizer of (3). Consider $f \in \mathcal{A}$. Then, we have

$$\begin{aligned}\mathcal{L}(C^\star) - \mathcal{L}(f) &= \int_0^T \left(C^\star(t) - f(t)\right)\Psi(t)dt = -\int_0^{T-\gamma} f(t)\Psi(t)dt + \int_{T-\gamma}^T (1 - f(t))\Psi(t)dt\\ &> \Psi(T-\gamma)\int_0^{T-\gamma} -f(t)dt + \Psi(T-\gamma)\int_{T-\gamma}^T 1 - f(t)dt\\ &= \Psi(T-\gamma)\left(\gamma - \int_0^T f(t)dt\right) = 0,\end{aligned} \tag{29}$$

where the strict inequality comes from the fact that $\Psi(t)$ is strictly increasing. Therefore, $C^\star$ is the unique maximizer of $\mathcal{L}$ and this completes the proof. □

The optimal formula obtained in (26) suggests a bang–bang profile for chemotherapy which is clinically known as an MTD protocol. It says that if one starts a chemotherapy cycle with a rest period and then administers the chemotherapy agent with the highest allowable dose from time $T - \gamma$ until the last day of treatment, it yields the smallest amount of tumor on the final day of the cycle.

The assertion of uniqueness in Theorem 1 implies that if we examine the chemotherapy profile proposed provided in (26), there is no opportunity for improving the chemotherapy based upon the information provided by the model in (1).

5. Numerical experiments

In this section we consider the optimal profile obtained in (26) and one other possible profile of chemotherapy for the PDE model (1). We also consider the case with no treatment. Utilizing data derived from clinical experiments involving various patients and employing the model on an actual brain image, we assess the outcomes of (1) across three distinct chemotherapy scenarios and validate the analytical result obtained in Theorem 1.

Note that one of the most significant aspects of (1) is its consideration of the heterogeneous structure of brain tissue. Experimental observations have shown that glioma cells migrate more rapidly in white matter than in the gray matter of the human brain. This observation justifies the consideration of $D_w = 5D_g$ [17]. The vascular makeup of the brain is varied, with capillary density notably higher in gray matter compared to white matter by approximately 3.5 times. Consequently, drug delivery to white matter is anticipated to be substantially lower than to gray matter. Due to this fact, we set $C_g = 3.5C_w$ and $C_w = 2.40 \times 10^{-2}$ day^{-1} in this paper [23].

We have established the duration of a chemotherapy cycle as 42 days, with a chemotherapy period within each cycle spanning 15 days [10]. This implies $T = 42$ days and the total chemotherapy effort $\gamma = 15$. We are examining 12 patients with varying biological parameters. In addition to the chemotherapy profile outlined in (26), we are exploring two alternative scheduling options for these patients, i.e., no treatment and uniform scheduling of treatment which means $C(t) \equiv 15/42$. Using the chemotherapy scenarios, we determine the solutions to (1) and compute the corresponding value of J. One can see the three different profiles of chemotherapy in Fig. 1.

The parameters used are reported in Table 1, sourced from [24]. We assumed that what has been reported in [24] for the diffusion is the invasion rate in the gray matter.

In our computations, we assume $K(\mathbf{x}) \equiv K$, thus scaling the solution of (1) by K allows us to set $K = 1$.

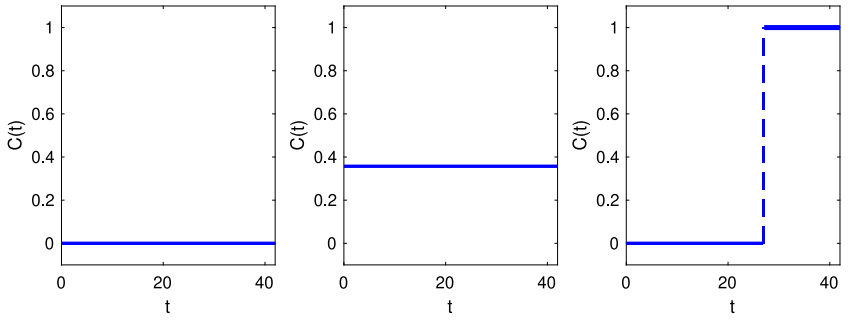

Fig. 1. Three different chemotherapy profiles: no treatment (left), uniform treatment (middle), and optimal scheduling (right), as described by (26).

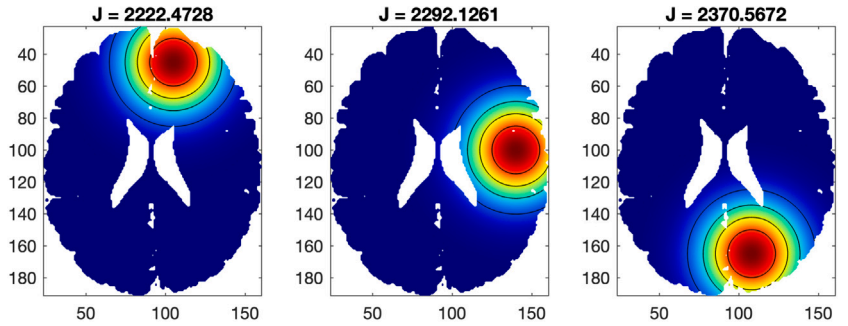

Fig. 2. Three different initial populations of tumor cells: (left) $\mathbf{x_0} = (105, 45)$ (middle) $\mathbf{x_0} = (140, 100)$ (right) $\mathbf{x_0} = (108, 165)$.

Table 1
Patient clinical data [24].

Patient	D_g (mm^2/day)	ρ (1/day)
1	5.05×10^{-2}	9.62×10^{-2}
2	2.06×10^{-2}	3.47×10^{-2}
3	7.59×10^{-2}	9.84×10^{-2}
4	2.16×10^{-2}	4.18×10^{-1}
5	2.44×10^{-2}	1.38×10^{-1}
6	2.96×10^{-2}	3.75×10^{-2}
7	1.34×10^{-1}	3.80×10^{-2}
8	3.46×10^{-2}	2.20×10^{-2}
9	1.80×10^{-2}	4.67×10^{-2}
10	1.49×10^{-1}	1.00×10^{-1}
11	5.17×10^{-2}	1.20×10^{-1}
12	5.29×10^{-3}	5.30×10^{-2}

We assume that initially the tumor is located in the frontal lobe, temporal lobe, or occipital lobe. Moreover, at first day treatment the tumor cells have a Gaussian initial distribution with a maximum cell density, a, at the center, $\mathbf{x}_0$, of the tumor; that is,

$$u_0(\mathbf{x}) = a \exp\left(-\frac{|\mathbf{x} - \mathbf{x}_0|^2}{b}\right),$$

where b is a measure of the spread of tumor cells [17]. See Fig. 2. Since we can experimentally track the profile of tumor cells above a certain detection level, we assume that this detection level is 80 percent of the carrying capacity. We also assume that the radius of the detected tumor is 15 mm, which is the average radius at which a tumor is identified [17, Section 11]. In view of these assumptions, we choose $a = 1$ and $b = (15)^2/(-\log(0.8))$ which implies that the initial tumor radius is 15 mm.

We compute the solution of (1) using three different chemotherapy profiles and calculate the corresponding values of J. The computations are performed on a brain image using an MRI dataset included in MRIcron, a cross-platform NIFTI format image viewer developed by Professor Chris Rorden and his group [25]. First, we use MATLAB to load the dataset and generate an axial view of the "ch2bet.nii" image, which has dimensions of $181 \times 217 \times 181$ mm^3, at the slice $z = 95$ mm. We then apply the segmentation approach described in [26] to identify grey matter (GM) and white matter (WM) regions. Following this, we prepare a triangular mesh for finite element analysis to solve Eq. (1) on the brain.

There different initial distributions of tumor cells considered in this paper are shown in Fig. 2. The location of the center of the initial tumor and its initial population size can be found in the figure.

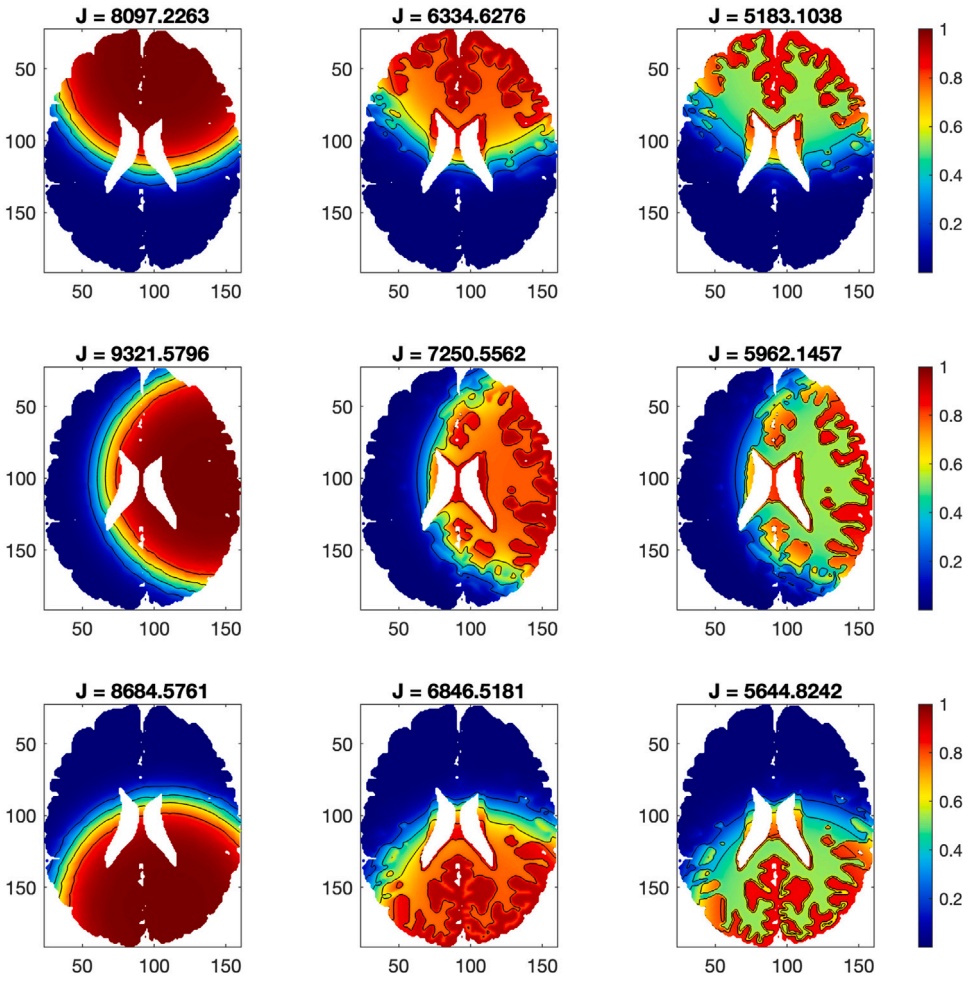

Fig. 3. Three different chemotherapy treatments are listed in columns, along with their corresponding tumor populations for three different tumor locations in rows, for patient 5.

To implement the finite element method for solving our PDE, we utilized MATLAB function `solvepde`. We performed computations for all patients listed in Table 1, considering three different initial tumor locations in the frontal lobe, temporal lobe, or occipital lobe, as mentioned in Fig. 2. However, we are only presenting the results for four different cases from various tumor grades while the remaining cases are presented in Appendix. The different tumor grades include high grade (high ρ and high D), intermediate grade (high ρ and low D or low ρ and high D), and low grade (low ρ and low D) [17].

We selected patient 10 as a high grade tumor, patients 5 and 7 as intermediate grade, and patient 8 as a low grade. However, it is important to note that the selection is not the only option; one can choose different patients. The results of our numerical computations at the last day of chemotherapy, i.e., $u(\mathbf{x}, T)$, are shown in Figs. 3–6. In these figures, the first column illustrates the tumor without treatment, the second column corresponds to uniform treatment, and the last one depicts the optimal treatment as defined in Eq. (26). Each row in the figures represents the results corresponding to one of the initial locations of the tumor mentioned above. The value of J for each case has been calculated and presented in the figures. The results for the other patients from Table 1 are presented in Appendix for the information of the reader.

All of these figures confirm the effect of treatment on tumor growth, while tumors can grow drastically without treatment. Our results show that the population size of the tumor is smaller with the chemotherapy profile suggested by (26) compared to the uniform dose delivery. This finding is in line with Theorem 1, which states that the treatment scheduling in (26) is minimal. However, one can observe that the efficacy of the optimal treatment in reducing tumor size on the last day of treatment, i.e., J, varies for tumors with different parameters and locations. This raises the question of which parameters, invasion rate and proliferation rate, correlate with the efficacy of the optimal treatment.

To address the question, we have plotted the relative difference $\left(J(0) - J(C^\star)\right)/J(0)$ with respect to ρ in Table 1 for different tumor locations in Fig. 7. The relative difference indicates the reduction in the size of the tumor in the last day of the optimal treatment compared to the size of the tumor without treatment. The linear regression line $a + b\rho$ is also plotted in the figure, and you can find the formula of the line for each tumor location in the caption of the figure.

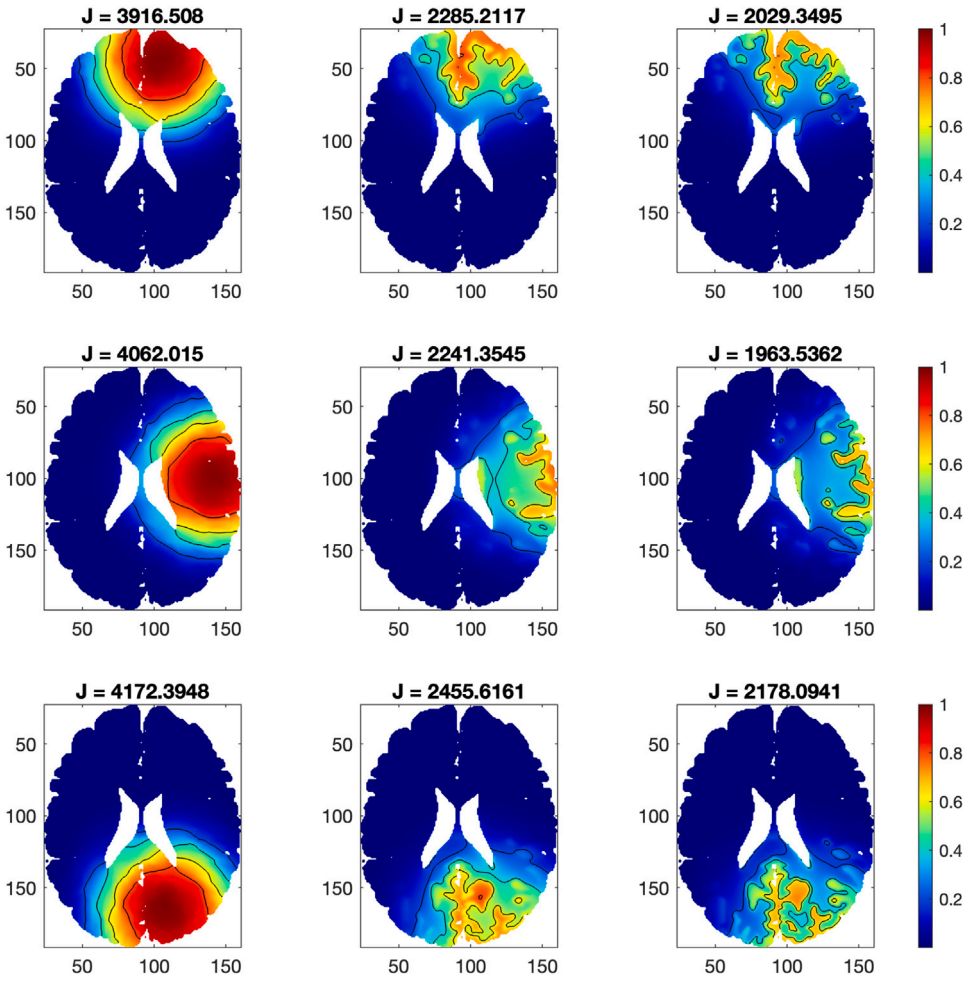

Fig. 4. Three different chemotherapy treatments are listed in columns, along with their corresponding tumor populations for three different tumor locations in rows, for patient 7.

6. Conclusions and discussions

In this study, we addressed the question of whether the MTD chemotherapy scheduling, a common practice in clinics, is optimal or if there is room for improvement. To do so, we used a reaction–diffusion PDE to model the evolution of the tumor in a cycle of chemotherapy. Considering the total population of tumor cells at the end of the cycle as our objective function, we formulated the question into a PDE-constrained optimization problem or an optimal control problem involving a PDE.

We have demonstrated that the optimization problem has a unique solution and have derived an analytical solution, which is rare in the context of PDE-constrained optimization. The optimal chemotherapy profile suggested by our results is a "bang–bang" increasing profile, as presented in Formula (26). Clinically, the optimal profile suggests starting the chemotherapy cycle with a rest period, followed by administering the medicine in the last days of the cycle at the highest allowable dose. This is what we known as MTD strategy in clinics for chemotherapy and a profile of it for a cycle can be found in [11, Figure 1] which is same as our optimal profile. This means that our results confirm and validate the MTD strategy in clinics. This result can be considered as a validation for the model (1) as it has been studied and improved during the past two decades, see for instance, [9].

Our numerical results validate our analytical results and confirm that the profile in (26) yields the smallest population size for tumor at the end of the treatment.

Fig. 7 shows a linear correlation between the proliferation rate ρ and the effectiveness of the optimal chemotherapy strategy in reducing tumor size at the end of treatment. This indicates that the optimal strategy is more successful in reducing tumor size for tumors with a higher proliferation rate compared to cases with no treatment. We observe a consistent linear correlation across all locations. However, it is worth noting that the slope of the linear regression may vary between different locations.

It appears that the influence of the invasion rate on the effectiveness of the optimal treatment is correlated in a more complex manner than what can be observed using our current model. This suggests the necessity of modifying the model (1). Nevertheless, we are confident that the model can be effectively utilized to analyze and enhance the current trends in radiotherapy for brain tumors. This could pave the way for new research in this direction.

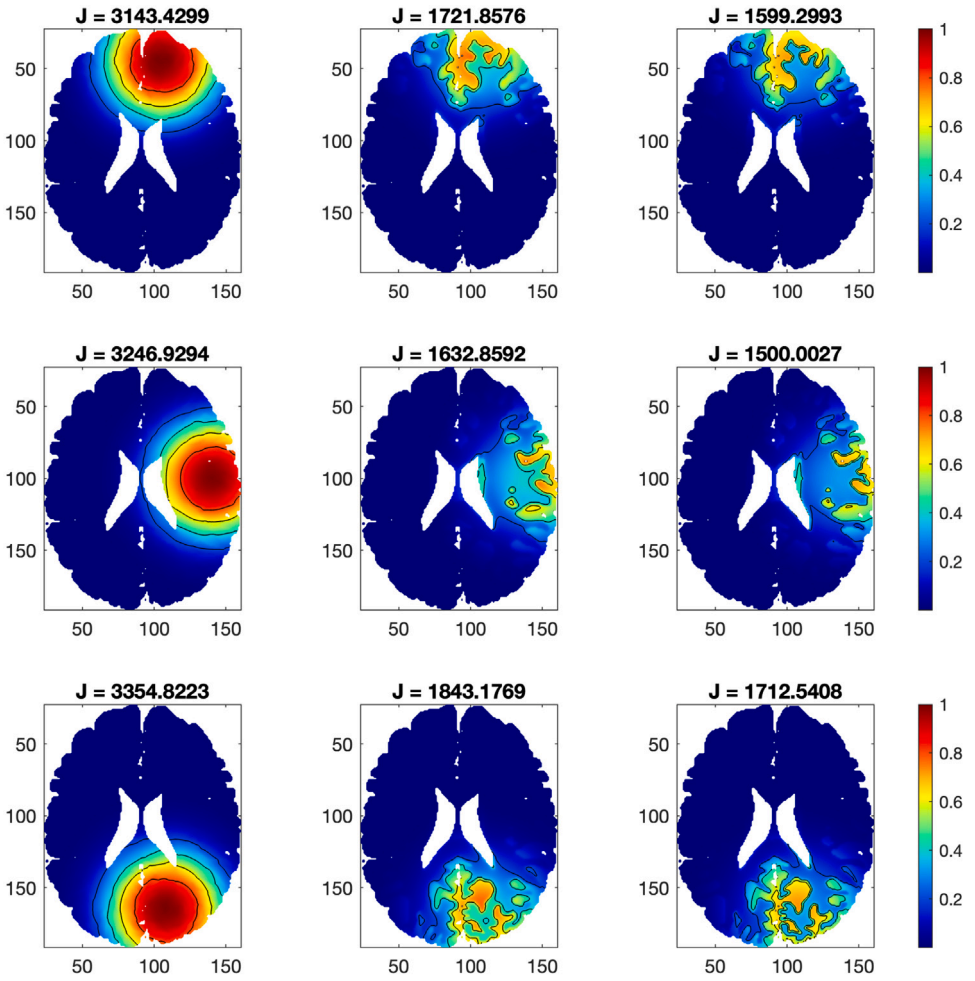

Fig. 5. Three different chemotherapy treatments are listed in columns, along with their corresponding tumor populations for three different tumor locations in rows, for patient 8.

CRediT authorship contribution statement

Chiu-Yen Kao: Conceptualization, Formal analysis, Funding acquisition, Investigation, Methodology, Project administration, Software, Supervision, Validation, Visualization, Writing – original draft, Writing – review & editing. **Seyyed Abbas Mohammadi:** Conceptualization, Formal analysis, Funding acquisition, Investigation, Methodology, Project administration, Resources, Software, Supervision, Validation, Visualization, Writing – original draft, Writing – review & editing. **Mohsen Yousefnezhad:** Conceptualization, Formal analysis, Funding acquisition, Investigation, Methodology, Project administration, Resources, Software, Supervision, Validation, Visualization, Writing – original draft, Writing – review & editing.

Declaration of competing interest

The authors declare that there are no conflicts of interest regarding the publication of this paper.

Data availability

Data will be made available on request.

Acknowledgment

The authors gratefully acknowledge Prof. Idriss Mazari from Université Paris-Dauphine, Université PSL, for generously sharing his insights and ideas regarding this paper.

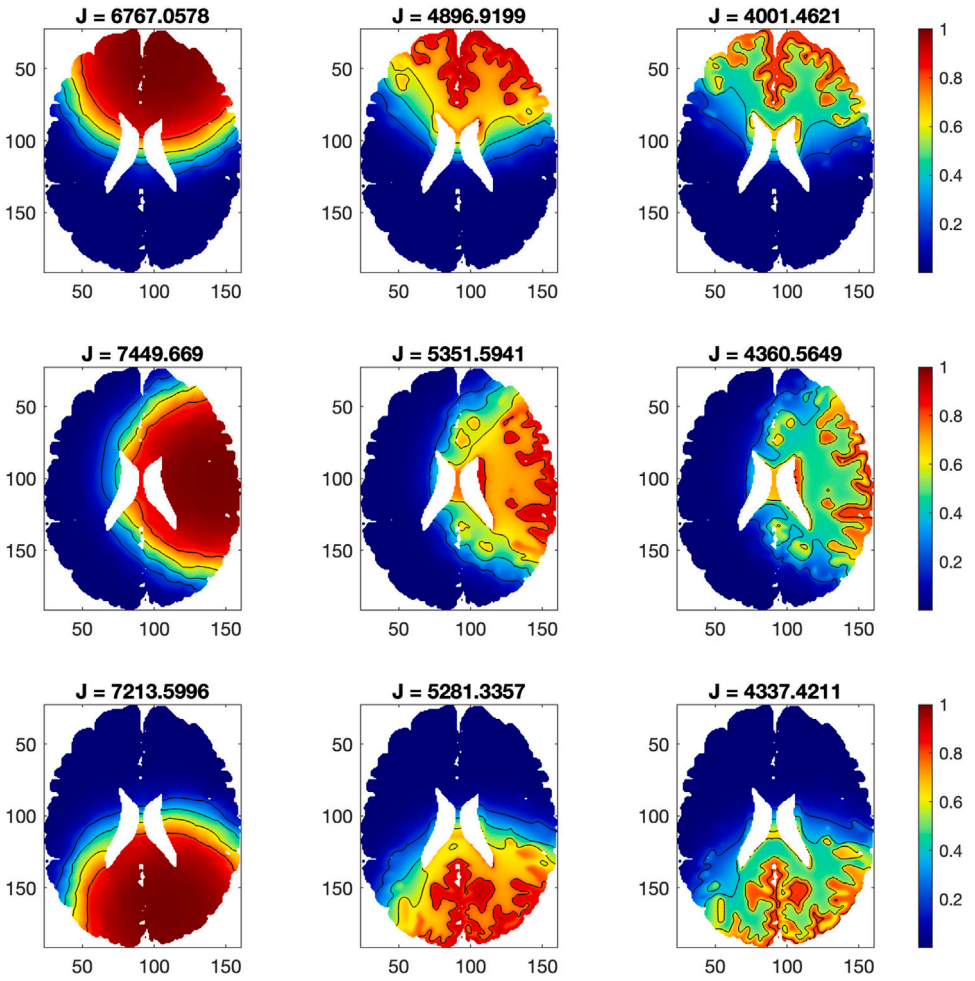

Fig. 6. Three different chemotherapy treatments are listed in columns, along with their corresponding tumor populations for three different tumor locations in rows, for patient 10.

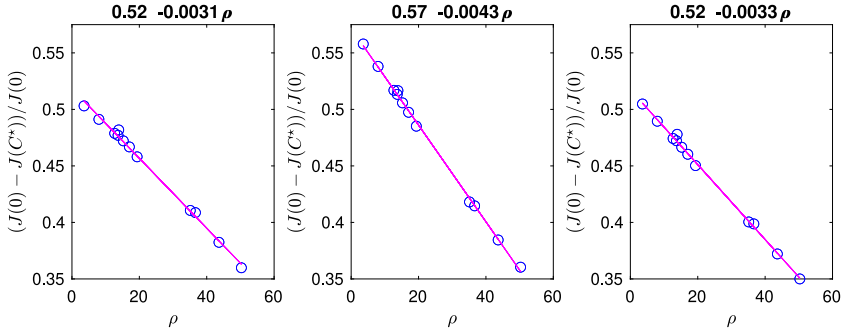

Fig. 7. The relative difference $\left(J(0) - J(C^*)\right)/J(0)$ with respect to ρ for different tumor locations: (left) $\mathbf{x_0} = (105, 45)$ (middle) $\mathbf{x_0} = (140, 100)$ (right) $\mathbf{x_0} = (108, 165)$.

Appendix

In this appendix, we will present the results of our numerical implementations for patients 1–4, 6,9, and 11–12 in Figs. 8–15 respectively.

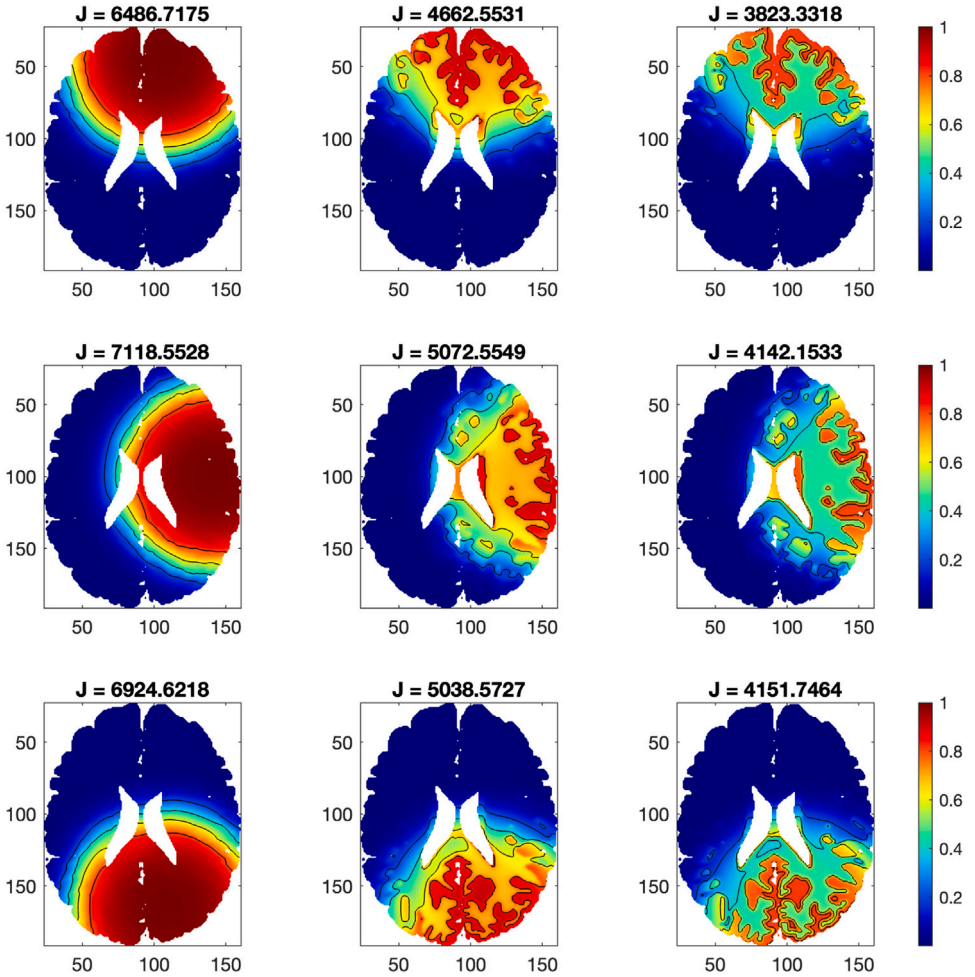

Fig. 8. Three different chemotherapy treatments are listed in columns, along with their corresponding tumor populations for three different tumor locations in rows, for patient 1.

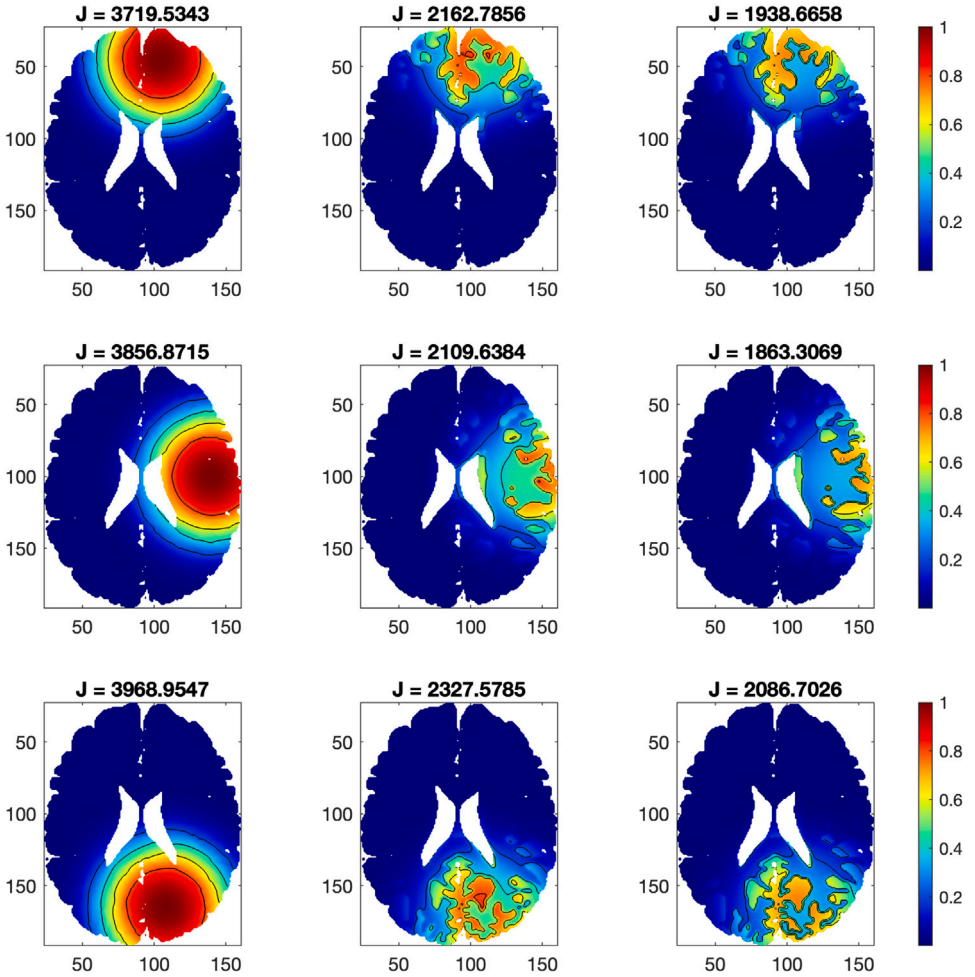

Fig. 9. Three different chemotherapy treatments are listed in columns, along with their corresponding tumor populations for three different tumor locations in rows, for patient 2.

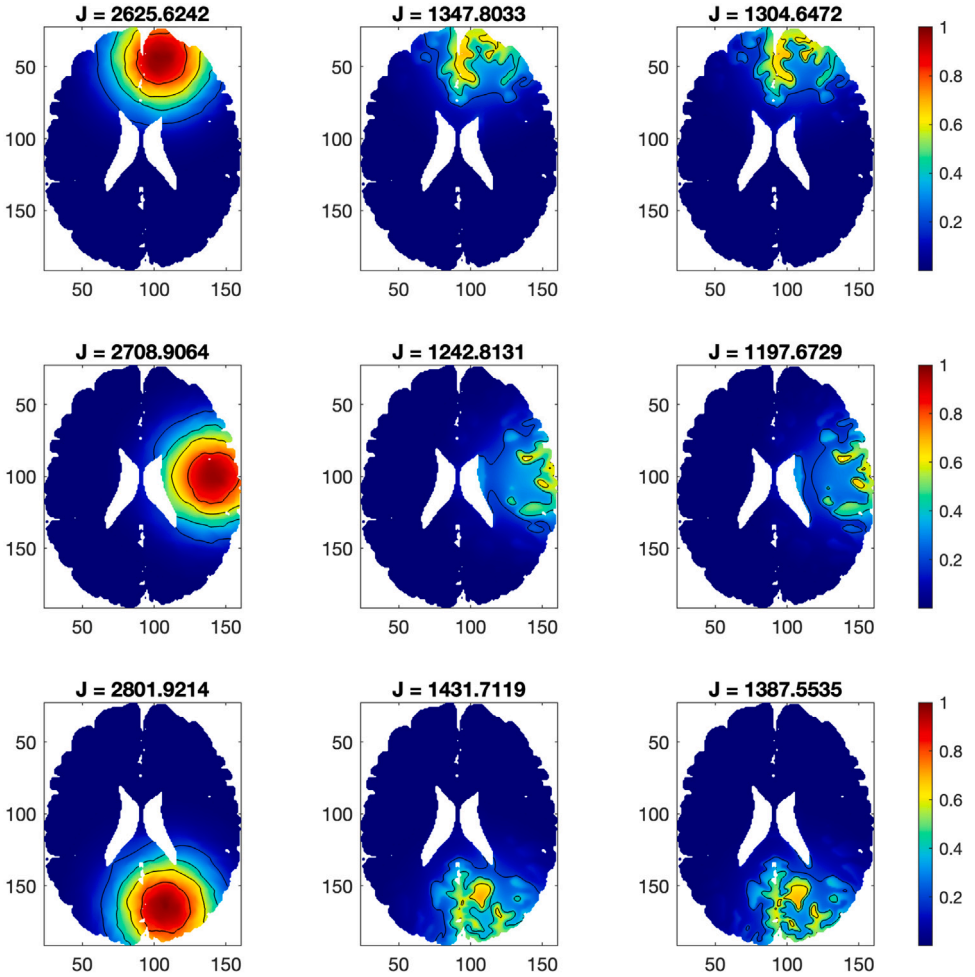

Fig. 10. Three different chemotherapy treatments are listed in columns, along with their corresponding tumor populations for three different tumor locations in rows, for patient 3.

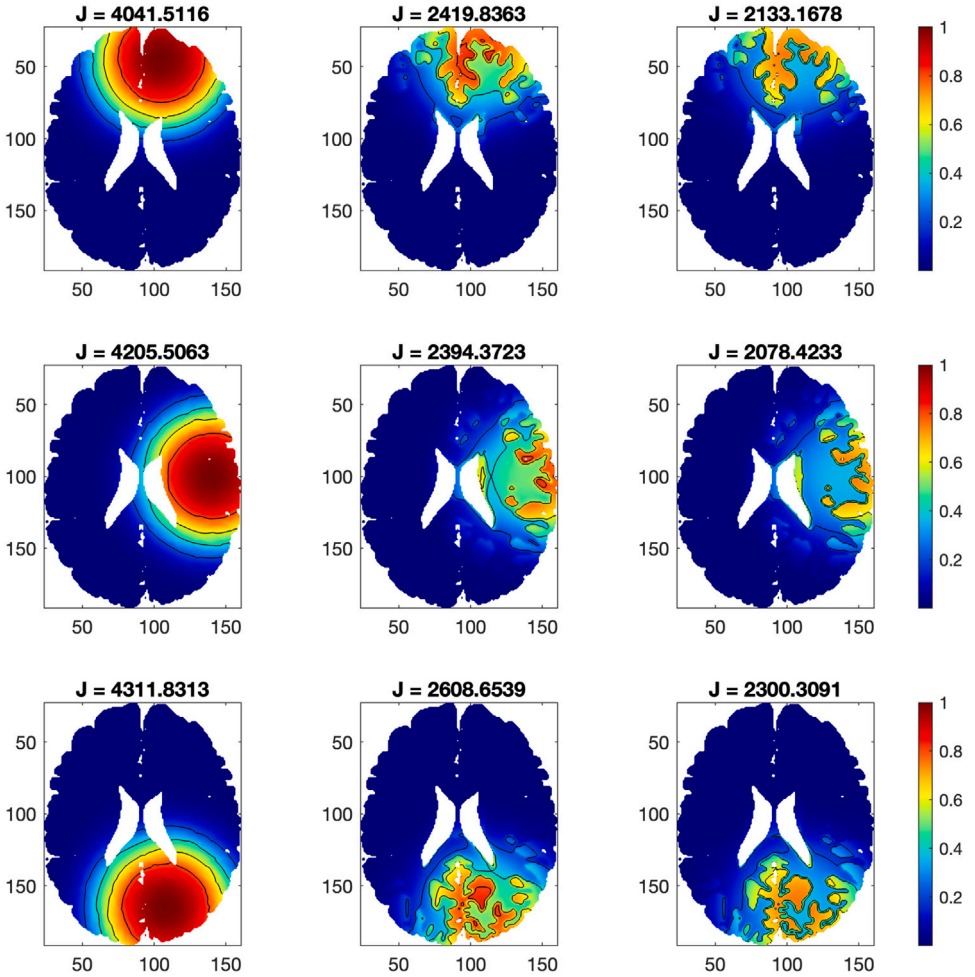

Fig. 11. Three different chemotherapy treatments are listed in columns, along with their corresponding tumor populations for three different tumor locations in rows, for patient 4.

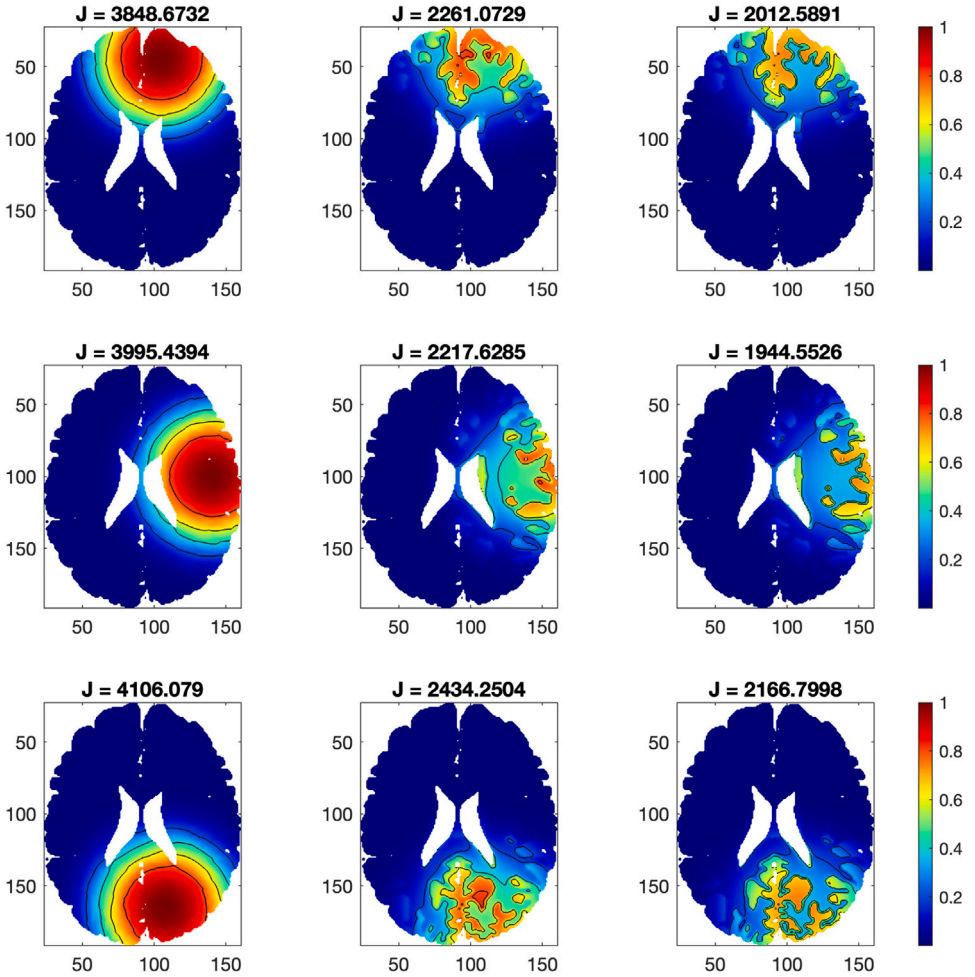

Fig. 12. Three different chemotherapy treatments are listed in columns, along with their corresponding tumor populations for three different tumor locations in rows, for patient 6.

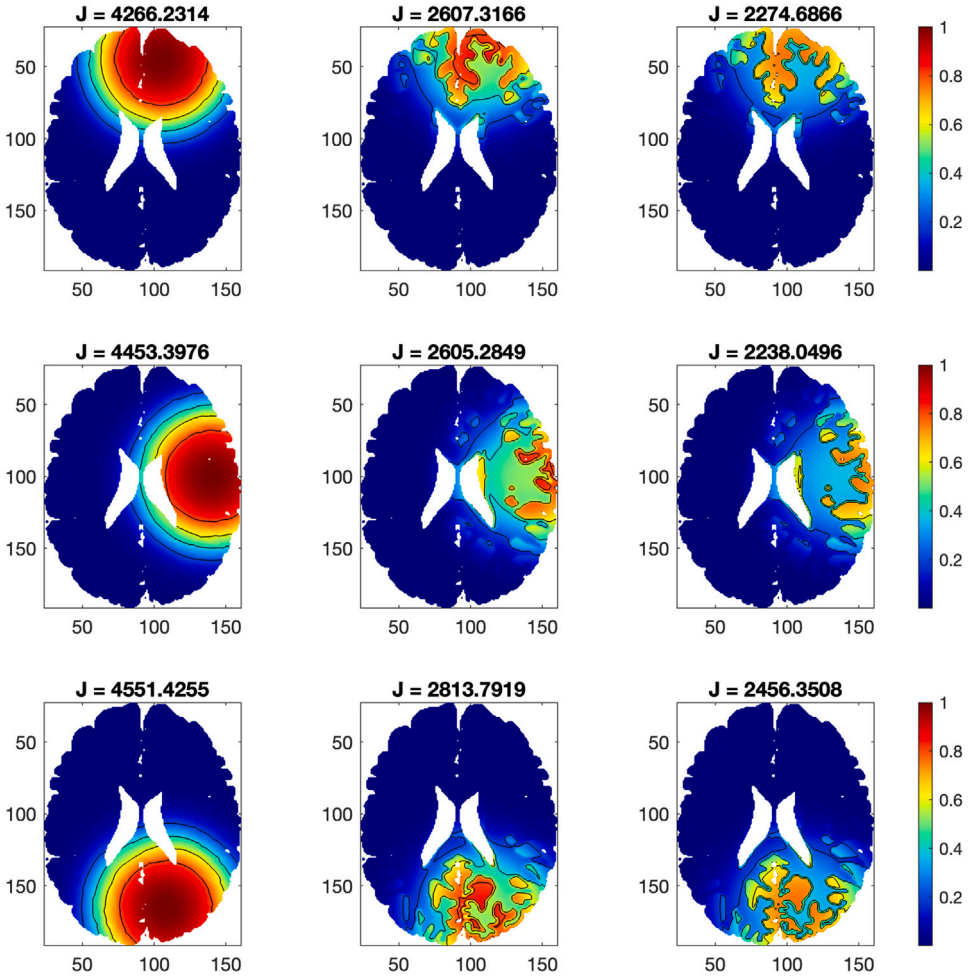

Fig. 13. Three different chemotherapy treatments are listed in columns, along with their corresponding tumor populations for three different tumor locations in rows, for patient 9.

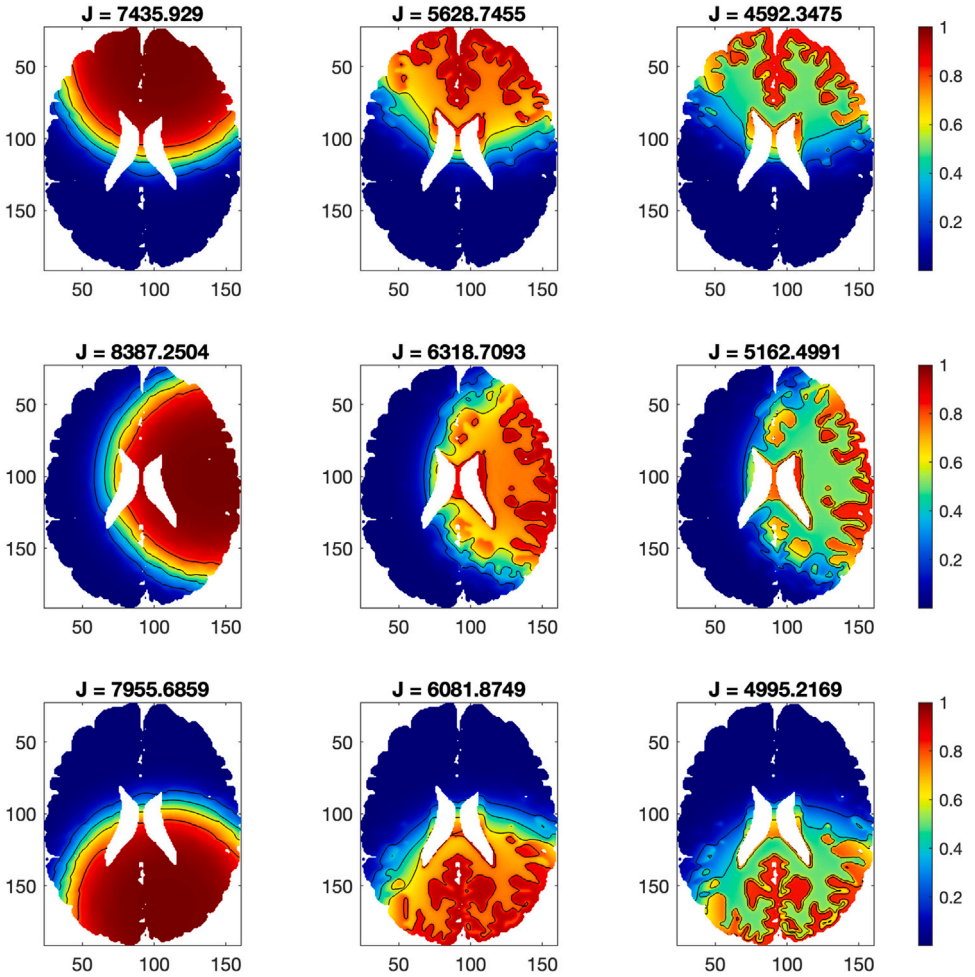

Fig. 14. Three different chemotherapy treatments are listed in columns, along with their corresponding tumor populations for three different tumor locations in rows, for patient 11.

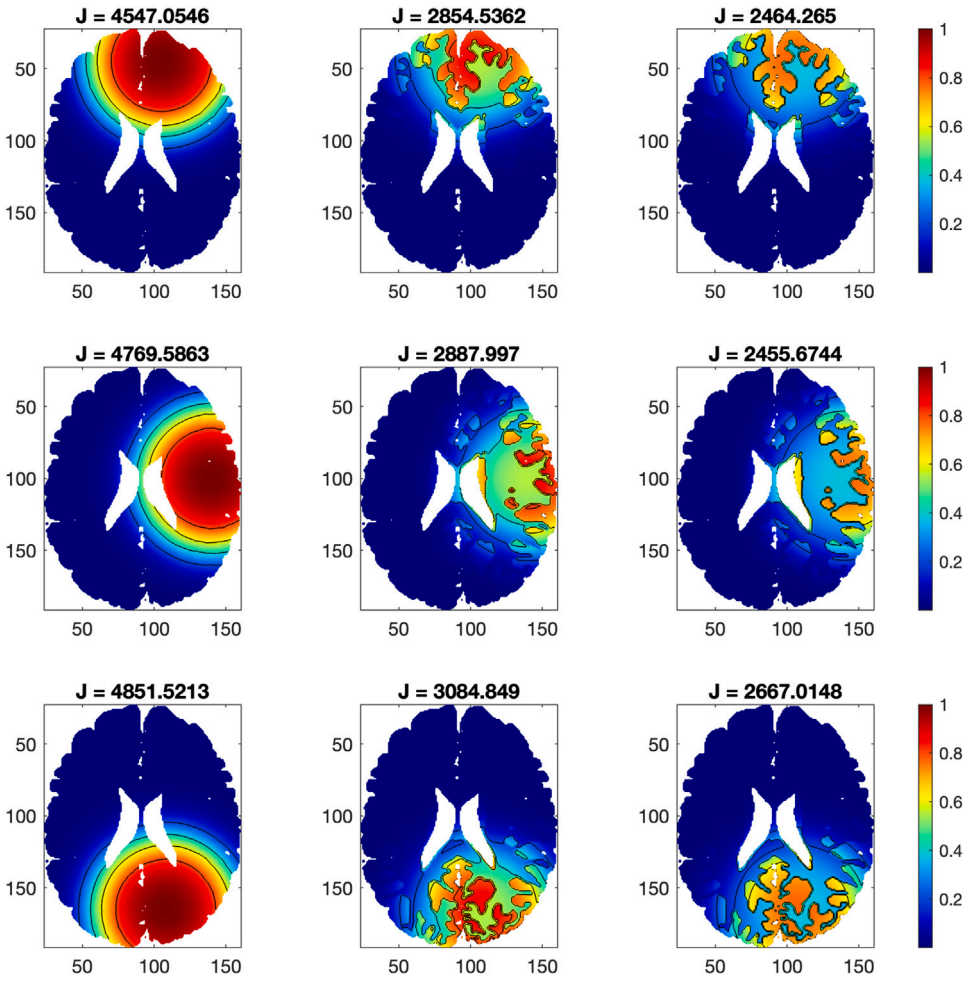

Fig. 15. Three different chemotherapy treatments are listed in columns, along with their corresponding tumor populations for three different tumor locations in rows, for patient 12.

References

[1] Alvord EC. Patterns of growth of gliomas. Am J Neuroradiol 1995;16(5):1013–7.
[2] Davis Mary Elizabeth. Glioblastoma: Overview of disease and treatment. Clin J Oncol Nurs 2016;20(5):S2.
[3] Holland Eric C. Glioblastoma multiforme: The terminator. Proc Natl Acad Sci 2000;97(12):6242–4.
[4] Alvarez-Arenas Arturo, Starkov Konstantin E, Calvo Gabriel F, Belmonte-Beitia Juan. Ultimate dynamics and optimal control of a multi-compartment model of tumor resistance to chemotherapy. Discrete Contin Dyn Syst Ser B 2019;24(5):2017.
[5] DeVita Vincent T, Lawrence Theodore S, Rosenberg Steven A. Cancer: principles & practice of oncology: primer of the molecular biology of cancer. Lippincott Williams & Wilkins; 2012.
[6] Powathil G, Kohandel M, Sivaloganathan S, Oza A, Milosevic M. Mathematical modeling of brain tumors: Effects of radiotherapy and chemotherapy. Phys Med Biol 2007;52(11):3291.
[7] World Health Organization, et al. WHO handbook for reporting results of cancer treatment. World Health Organization; 1979.
[8] Therasse Patrick, Arbuck Susan G, Eisenhauer Elizabeth A, Wanders Jantien, Kaplan Richard S, Rubinstein Larry, et al. New guidelines to evaluate the response to treatment in solid tumors. J Natl Cancer Inst 2000;92(3):205–16.
[9] Jackson Trachette, Komarova Natalia, Swanson Kristin. Mathematical oncology: Using mathematics to enable cancer discoveries. Amer Math Monthly 2014;121(9):840–56.
[10] Swanson Kristin R, Alvord Ellsworth C, Murray JD. Quantifying efficacy of chemotherapy of brain tumors with homogeneous and heterogeneous drug delivery. Acta Biotheoretica 2002;50(4):223–37.
[11] Tracqui P, Cruywagen GC, Woodward DE, Bartoo GT, Murray JD, Alvord Jr EC. A mathematical model of glioma growth: The effect of chemotherapy on spatio-temporal growth. Cell Prolif 1995;28(1):17–31.
[12] Bratus Alexander, Samokhin Igor, Yegorov Ivan, Yurchenko Daniil. Maximization of viability time in a mathematical model of cancer therapy. Math Biosci 2017;294:110–9.
[13] Ledzewicz U, Schättler H. A review of optimal chemotherapy protocols: from MTD towards metronomic therapy. Math Model Nat Phenom 2014;9(4):131–52.
[14] Ledzewicz Urszula, Schättler Heinz, Gahrooi M Reisi, Dehkordi S Mahmoudian. On the MTD paradigm and optimal control for multi-drug cancer chemotherapy. Math Biosci Eng 2013;10(3):803–19.

[15] Moradi Hamed, Vossoughi Gholamreza, Salarieh Hassan. Optimal robust control of drug delivery in cancer chemotherapy: A comparison between three control approaches. Comput Methods Programs Biomed 2013;112(1):69–83.
[16] Yousefnezhad Mohsen, Kao Chiu-Yen, Mohammadi Seyyed Abbas. Optimal chemotherapy for brain tumor growth in a reaction-diffusion model. SIAM J Appl Math 2021;81(3):1077–97.
[17] Murray James D. Mathematical biology, interdisciplinary applied mathematics. New York, NY: Springer; 2004, https://link.springer.com/book/10.1007/b98869.
[18] Tröltzsch Fredi. Optimal control of partial differential equations: Theory, methods, and applications, vol. 112, American Mathematical Soc.; 2010.
[19] Evans Lawrence C. Partial differential equations, vol. 19, American Mathematical Society; 2022.
[20] Filippov Aleksei Fedorovich. Differential equations with discontinuous righthand sides: control systems, vol. 18, Springer Science & Business Media; 2013.
[21] Roubíček Tomáš. Nonlinear partial differential equations with applications, vol. 153, Berlin: Springer Science & Business Media; 2013.
[22] Finotti Heather, Lenhart Suzanne, Van Phan Tuoc. Optimal control of advective direction in reaction-diffusion population models. Evol Equ Control Theory 2012;1(1):81–107.
[23] Swanson Kristin R, Alvord Jr Ellsworth C, Murray JD. A quantitative model for differential motility of gliomas in grey and white matter. Cell Prolif 2000;33(5):317–29.
[24] Corwin David, Holdsworth Clay, Rockne Russell C, Trister Andrew D, Mrugala Maciej M, Rockhill Jason K, et al. Toward patient-specific, biologically optimized radiation therapy plans for the treatment of glioblastoma. PLoS One 2013;8(11):e79115.
[25] Rorden Chris. 2020, MRIcron, Date-Added=2014-09-05, Date-Modified=2020-07-29, https://www.nitrc.org/projects/mricron.
[26] Li Chunming, Kao Chiu-Yen, Gore John C, Ding Zhaohua. Minimization of region-scalable fitting energy for image segmentation. IEEE Trans Image Process 2008;17(10):1940–9.